Infrared Physics & Technology 53 (2010) 348–357

Contents lists available at ScienceDirect

Infrared Physics & Technology

journal homepage: www.elsevier.com/locate/infrared

Research on thermal wave processing of lock-in thermography based on analyzing image sequences for NDT

Liu Junyan [a,*], Wang Yang [a], Dai Jingmin [b]

[a] School of Mechatronics Engineering, Harbin Institute of Technology, Harbin, PR China
[b] School of Electronic Engineering and Automation, Harbin Institute of Technology, Harbin, PR China

ARTICLE INFO

Article history:
Received 10 October 2009
Available online 10 June 2010

Keywords:
Lock-in thermography
Non-destructive testing
Image sequence
Thermal wave signal processing

ABSTRACT

Lock-in thermography, an active IR thermography technique for NDT, is based on propagation and reflection of thermal waves which are launched from the surface into the inspected component by absorption of modulated radiation. In this paper, thermal wave image sequences were sampled by a Cedip JADE MWIR 550 FPA infrared camera. Thermal wave signal processing algorithms are investigated to obtain information on subsurface defects. The Fourier transform, four-point correlation, and digital lock-in correlation algorithms are applied to extract the amplitude and phase of thermal wave's harmonic component. A novel method called the time constant method (TCM) is proposed to analyze subsurface defects by using lock-in thermography. The experimental results confirm the thermal wave signal processing algorithms' efficiency on subsurface defect detection.

1. Introduction

Thermography is a non-destructive evaluation technique that measures the surface temperature variations in response to induced energy. The energy creates a temperature contrast at material discontinuities that can be detected by an infrared camera [1]. Since the early 1960s, infrared thermography (IRT) has been successfully used as a NDT&E technique in many applications. Thermography is gaining more acceptance as a fast non-contact and large area visualizing inspection technique primarily due to the recent advances in data acquisition and analysis systems [2].

Presently, two types of active thermal non-destructive techniques are predominantly in use: pulsed thermography and modulated lock-in thermography. In pulsed thermography, the test material is warmed with a short duration excited energy pulse, e.g., flash lamp, laser beam and ultrasonic heating, etc. An infrared camera is applied to monitor the temporal evolution of surface temperature. The surface temperature gradients on the specimen are helpful to localize the subsurface defect on such material. However, the surface temperature gradients depend not only on subsurface defects, but also on local variations of emissivity as well as non-uniform heating [3]. The phase pulsed thermography (PPT) combines the advantages of pulsed thermography and modulated lock-in thermography simultaneously without sharing their traditional drawbacks [4]. Lock-in thermography (LT) has been applied successfully in non-destructive test and evaluation for many years. LT utilizes periodic harmonic heat to excite the sample surface at low peak power, which enables us to derive amplitude and phase angle from reflection thermal wave [5]. Also the phase angle has the advantage of being less sensitive to the local variations of illumination or surface emissivity.

Lock-in principle is the technique of choice, if the signal has to be extracted from statistical noise [6]. This work focuses on theoretical analysis of lock-in thermography. Three thermal wave processing algorithms are investigated to extract the amplitude and phase angle of thermal wave's harmonic component. The amplitude or phase image is used for non-destructive subsurface defect detection in solids. By means of the mathematical analysis on the thermal wave in transient state, a new transient thermal wave processing algorithm is proposed to detect subsurface defects.

2. Theory

The excitation harmonic heat flux is represented by a time varying sinusoidal equation n lock-in thermography, given by,

$$q_0(t) = \frac{q_{\max}}{2}(1 - \cos(2\pi f_e t)) \quad (1)$$

where $q_0(t)$ is the heat flux density, $q_{\max}$ is the maximum of heat flux density, f_e is the modulated frequency of external excitation heat flux and t is the time.

An opaque, homogenous and infinitely large plate of finite thickness (L) is considered. The plate is surrounded by air, and the front surface of plate is heated by harmonic heat flux (shown in Fig. 1).

* Corresponding author. Tel.: +86 451 86403380; fax: +86 451 86402755.
E-mail address: ljywlj@hit.edu.cn (J. Liu).

1350-4495/$ - see front matter
doi:10.1016/j.infrared.2010.06.002

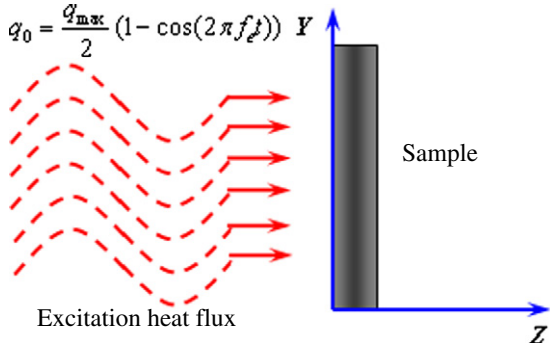

Fig. 1. The external heat flux transiting in solid.

The temperature distribution is obtained by Fourier law of heat conduction [7].

$$\frac{\partial^2 T(Z,t)}{\partial Z^2} = \frac{k}{\rho c}\frac{\partial T(Z,t)}{\partial t} \tag{2}$$

where $T(Z, t)$ is the temperature, k is the thermal conductivity, ρ is the density and c is the specific heat, and Z stands for the space coordinate.

When the solid is heated, the heat flux can be considered as two parts: constant heat flux $q_{max}/2$ which produces the temperature increased; harmonic heat flux $q_{max}/2 \times \cos(2\pi f_e t)$ which produces harmonic thermal modulation. The solution of $T(Z, t)$ is achieved by considering boundary conditions at the irradiated sample surface ($Z = 0$) and opposite face ($Z = L$).

The steady state solution of $T(Z, t)$ is expressed in the following equation [5]:

$$\begin{aligned} T(Z,t)_S &= A_s \exp\left(-Z\sqrt{\frac{i2\pi f_e \rho c}{k}}\right)\exp(i2\pi f_e t) \\ &= A_s \exp\left(\frac{-Z}{\Lambda}\right)\exp\left[i(2\pi f_e t) - \frac{Z}{\Lambda}\right] \end{aligned} \tag{3}$$

where $T(Z, t)_S$ is the harmonic temperature distribution in steady state, As is the amplitude of harmonic temperature, and $\Lambda = \sqrt{\frac{k}{\pi f_e \rho c}}$ represents the thermal diffusion length.

The $T(Z, t)_T$ which is the temperature variation in transient state follows the partial differential equations due to constant heat flux heated

$$\rho c\frac{\partial T(Z,t)_T}{\partial t} = \frac{q_{max}}{2} - \frac{T(Z,t)_T - T_{am}}{R_{th}} \tag{4}$$

where T_{am} is the ambient temperature, and the R_{th} is the thermal resistance of sample material.

The transient solution of $T(Z, t)_T$ of Eq. (4) is written in the following equation:

$$T(Z,t)_T = T_{am} + \Delta T(1 - e^{-t/\tau}) \tag{5}$$

where $\tau = \rho c R_{th}$ is called time constant, and $\Delta T = q_{max}/2 \times R_{th}$.

The solution of $T(Z, t)$ is obtained by Eq. (3) and Eq. (5) – given by,

$$T(Z,t) = T(Z,t)_T + T(Z,t)_S \tag{6}$$

Fig. 2 shows the sample surface temperature variation with different time constant.

In Fig. 2, the surface temperature increases rapidly due to thermal accumulation of constant heat flux in the given computational times. The temperature includes alternating components with harmonic heat flux action. The time constant determines how fast? the surface temperature achieves the steady state.

3. Thermal wave signal processing algorithms

3.1. Fourier transforms method (FTM)

Fourier transform method is a powerful/popular tool to calculate the amplitude and phase angle of thermal wave signal harmonic components [8]. This method is available prior to calculate the amplitude and phase of thermal wave signal on the off-line.

The Fourier transform of thermal images sequence is given in Eq. (7) at the modulated frequency f_e which is called lock-in frequency:

$$\begin{aligned} F_K(x,y) &= \sum_{n=0}^{N-1}\left[F_n(x,y)\cdot\exp\left(-j\frac{2\pi Kn}{N}\right)\right] \\ &= \sum_{n=1}^{N}\left[F_n(x,y)\cdot W_N^{(n-1)(K-1)}\right] \quad W_N = \exp\left(-j\frac{2\pi}{N}\right) \\ K &= 1,2,\ldots,N \end{aligned} \tag{7}$$

where $F_K(x, y)$ are the Fourier transforms of thermal image sequence, $F_n(x, y)$ is the thermal image sequence, N is the number of sample per lock-in period, and K is the digital frequency.

In order to extract thermal wave at the lock-in frequency, the digital frequency K is given in the following equation [9]:

$$K = N\frac{f_e}{f_s} + 1 \tag{8}$$

where f_s is the frame rate.

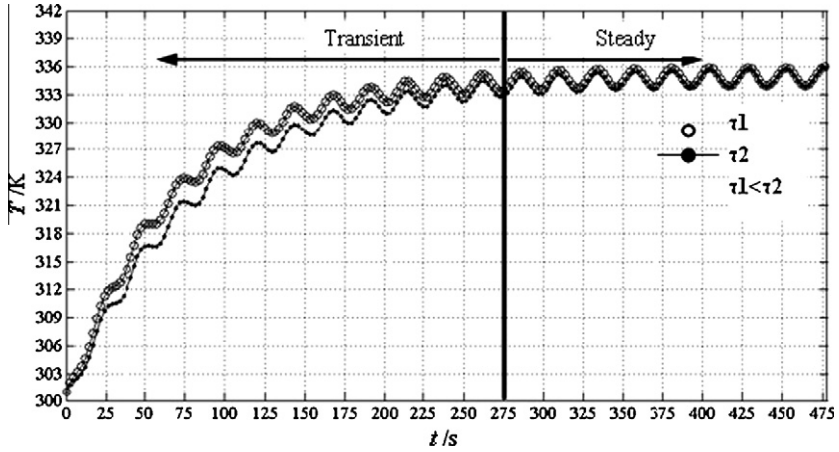

Fig. 2. The temperature variation and the effect of the constant time.

The amplitude and phase angle of thermal wave are obtained by,

$$A_s = \sqrt{[\mathrm{Re}(F_K(x,y))]^2 + [\mathrm{Im}(F_K(x,y)]^2} \tag{9}$$

$$\varphi = a\tan\left(\frac{\mathrm{Im}(F_K(x,y))}{\mathrm{Re}(F_K(x,y))}\right) \tag{10}$$

where A_s is the amplitude of thermal wave signal, φ is the phase angle of thermal wave signal.

In order to analyze the performance of the thermal wave signal Fourier transforms, we can assume that the surface temperature variation of Eq. (6) has been solved for the carbon steel ANSI 1045 as specimen (i.e., $f_e = 0.12$ Hz, $A_s = 2$, $\tau_1 = 6$, $\tau_2 = 12$, $\varphi_1 = 30°$ and $\varphi_2 = 60°$). The surface temperature variation of sample is shown in Fig. 3. The Fourier transform amplitude–frequency and phase–frequency properties of surface temperature are shown in Fig. 4.

In Fig. 4, the transient surface temperature is seriously affected by the amplitude of the surface temperature at the modulated frequency, and the amplitude calculated of surface temperature in transient is larger than in steady state. The surface temperature in the transient state, however, is hardly influenced on phase of surface temperature at modulated frequency, and the phase of surface temperature in the steady state is accurately obtained by FTM in the transient state.

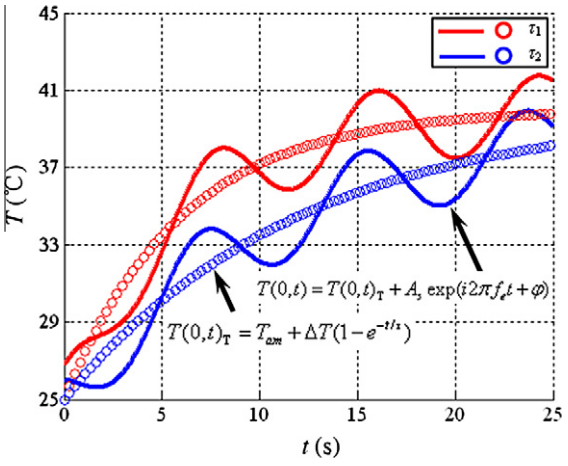

Fig. 3. Surface temperature variation.

3.2. Four-point correlation method (FPCM)

Four-point correlation method was firstly proposed by Busse et al. [5] in 1992. This method uses four equidistant surface temperature (thermal wave) data points S_1–S_4, the amplitude and phase of thermal wave signal are given by [4]:

$$\varphi = \arctan\frac{S_3(X_1) - S_1(X_1)}{S_4(X_1) - S_2(X_1)} \tag{11}$$

$$A_s = \sqrt{(S_3(X_1) - S_1(X_1))^2 + (S_4(X_1) - S_2(X_1))^2} \tag{12}$$

In order to reduce the noise, more thermal wave data points were averaged instead of four data points. The four-point correlation principle provides a method to calculate the amplitude and phase angle fast in lock-in thermography, show in Fig. 5.

3.3. Digital lock-in correlation method (DLCM)

The digital lock-in correlation method is a typical narrow band correlation. It evaluates only to the basic harmonic of the thermal wave signal which usually carries the dominant information, whereas higher harmonics are suppressed. The digital lock-in correlation method can be realized by using a synchronous correlation between thermal wave signal and a reference harmonic function. The sine/cosine correlation has the decisive advantage that it allows one to exactly consider the phase of the thermal wave signal after the measurement. Two-channel correlation which includes two reference sine/cosine functions respectively is used. The first channel calculates the component of thermal wave signal in-phase by sine function, and other channel calculates the component in-phase by cosine function.

$$c(n)^{0°} = 2\sin\left(\frac{2\pi(n-1)}{N}\right) \quad n = 1,2,\ldots,N \tag{13}$$

$$c(n)^{-90°} = 2\cos\left[\frac{2\pi(n-1)}{N}\right] \quad n = 1,2,\ldots,N \tag{14}$$

$$S^{0°} = \frac{c_s}{P_s N}\sum_{i=1}^{P_s}\sum_{n=1}^{N}\left[F_{i;n}(x,y)\cdot 2\cdot\sin\left(\frac{2\pi(n-1)}{N}\right)\right] \tag{15}$$

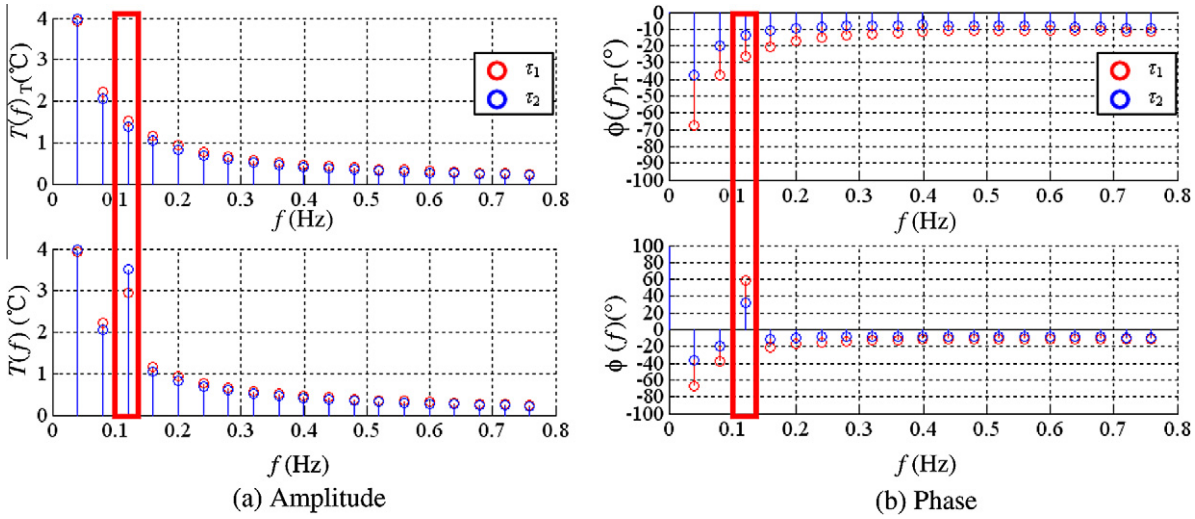

Fig. 4. Amplitude and phase characteristic of thermal wave signal.

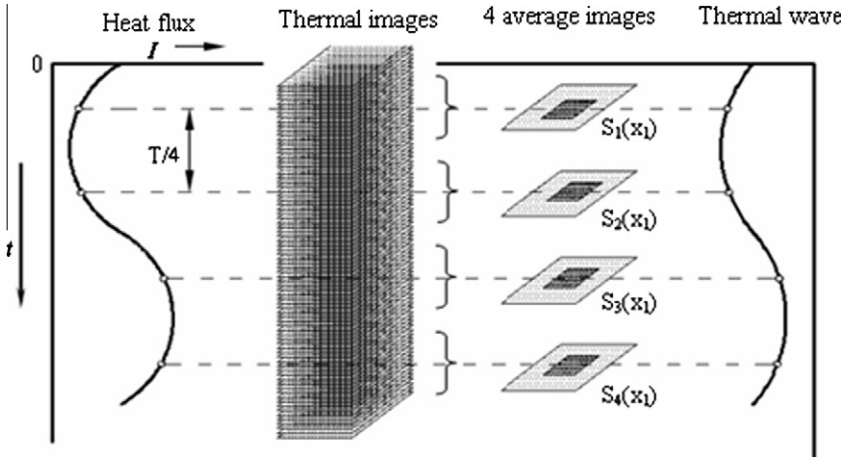

Fig. 5. Four-point correlation principle in lock-in thermography.

$$S^{-90^\circ} = \frac{c_s}{P_s N}\sum_{i=1}^{P_s}\sum_{n=1}^{N}\left[F_{i;n}(x,y)\cdot -2\cdot\cos\left(\frac{2\pi(n-1)}{N}\right)\right] \tag{16}$$

where $c(n)^{0^\circ}$ is the reference sine function, $c(n)^{-90^\circ}$ is the reference cosine function, S^{0° is the component of thermal signal by sin-function, and S^{-90° is the -90° phase shifted to the S^{0°, cs is the scaling factor, $F_{i;n}(x, y)$ is the thermal wave image for given period, and P_s is the number of modulation period.

The amplitude and phase angle of thermal wave signal can be obtained by the following equations.

$$A_s = \sqrt{(S^{0^\circ})^2 + (S^{-90^\circ})^2} \tag{17}$$

$$\varphi = a\tan\left(\frac{S^{-90^\circ}}{S^{0^\circ}}\right) \tag{18}$$

Fig. 6 shows the digital lock-in correlation method principle.

3.4. Time constant method (TCM)

Time constant method in lock-in thermography is firstly proposed in this paper, which calculates the ratio between modulation periodic and thermal wave time constant in transient state. The surface temperature can be calculated by Eq. (6) at time $t = t_0$, $t = t_0 + T_e$ and $t = t_0 + 2T_e$ respectively.

$$T(0,t_0) = T_{am} + \Delta T(1 - e^{-t_0/\tau}) + A_s\exp(i2\pi f_e t_0) \tag{19}$$

$$T(0,t_0+T_e) = T_{am} + \Delta T(1 - e^{-(t_0+T_e)/\tau}) \tag{20}$$

$$+ A_s\exp\left(i2\pi f_e(t_0+T_e)\right) \tag{21}$$

$$T(0,t_0+2T_e) = T_{am} + \Delta T(1 - e^{-(t_0+2T_e)/\tau}) + A\exp\left(i2\pi f_e(t_0+2T_e)\right) \tag{22}$$

where $T_e = 1/f_e$ is the modulation period.

So the following expressions can be obtained.

$$\Delta T(0,T_e) = T(0,t_0+T_e) - T(0,t_0) = \Delta T e^{-t_0/\tau} - \Delta T e^{-(t_0+T_e)/\tau} \tag{23}$$

$$\Delta T(0,2T_e) = T(0,t_0+2T_e) - T(0,t_0) = \Delta T e^{-t_0/\tau} - \Delta T e^{-(t_0+2T_e)/\tau} \tag{24}$$

$$\Delta^2 T(0,T_e) = \Delta T(0,2T_e) - \Delta T(0,T_e) = \Delta T e^{-t_0/\tau}e^{-T_e/\tau} - \Delta T e^{-t_0/\tau}e^{-T_e/\tau}e^{-T_e/\tau} \tag{25}$$

where $\Delta T(0, T_e)$ is the temperature difference in one modulation period, and $\Delta T(0, 2T_e)$ is the temperature difference in two modulation period.

Eqs. (26) and (27) can be obtained by taking logarithm of Eqs. (24) and (25).

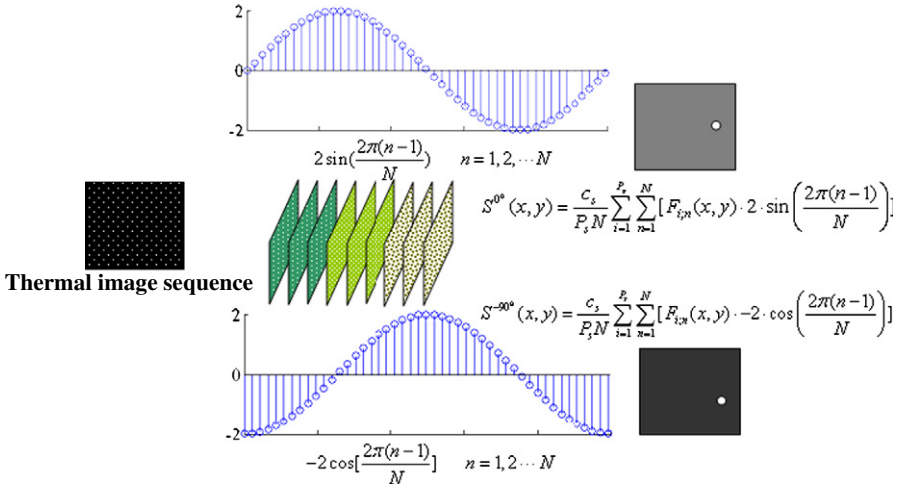

Fig. 6. Digital lock-in correlation principle in lock-in thermography.

$$\ln[\Delta T(0,T_e)] = \ln \Delta T - \frac{t_0}{\tau} + \ln(1 - e^{-T_e/\tau}) \quad (26)$$

$$\ln[\Delta^2 T(0,T_e)] = \ln \Delta T - \frac{t_0}{\tau} - \frac{T_e}{\tau} + \ln(1 - e^{-T_e/\tau}) \quad (27)$$

Eq. (28) is obtained by subtraction between Eqs. (26) and (27)

$$\frac{T_e}{\tau} = \ln[\Delta T(0,T_e)] - \ln[\Delta^2 T(0,T_e)] \quad (28)$$

The ratio between modulation period and time constant of surface temperature in transient state is applied to detect the subsurface defect in lock-in thermography. In order to reduce the noise, more thermal wave data points are averaged? three data points. The principle of TCM is showed in Fig. 7.

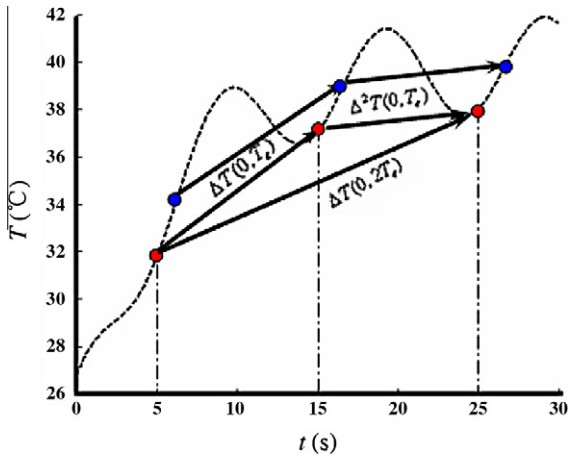

Fig. 7. Time constant method of thermal wave signal in transient state.

4. Experimental setup

ANSI 1045 steel plate with bottom holes and CFRP sheet faces honeycomb with different model subsurface defects are used as the specimens in this work. Fig. 8 illustrates the structure of all the specimens.

A schematic diagram of experimental system set up is shown in Fig. 9. Two lamps are used to supply external excitation heating source. Signal source generates a sine-wave type signal to drive the power amplifier changing the light heat flux according to harmonic sine-wave signals. The surface temperature (thermal wave) is recorded by an IR camera to form thermal image sequences? and the thermal wave signal processing algorithms are used to analyze thermal image sequence off-line in lock-in thermography. Fig. 10 illustrates the setup of the experimental system, and Fig. 11 shows the thermal wave signal processing software self-developed by authors. The experimental parameters are listed in Tables 1 and 2.

5. Results and discussion

Fig. 12a–c shows the amplitude images of the ANSI 1045 steel plate specimen, using FTM, FPCM and DLICM at modulation frequency f_e = 0.12 Hz, respectively. Compared with FPCM and DLICM, experimental results show that the FTM has higher capability to detect the subsurface defect in an amplitude image due to the lager amplitude difference between defective regions and non-defective ones.

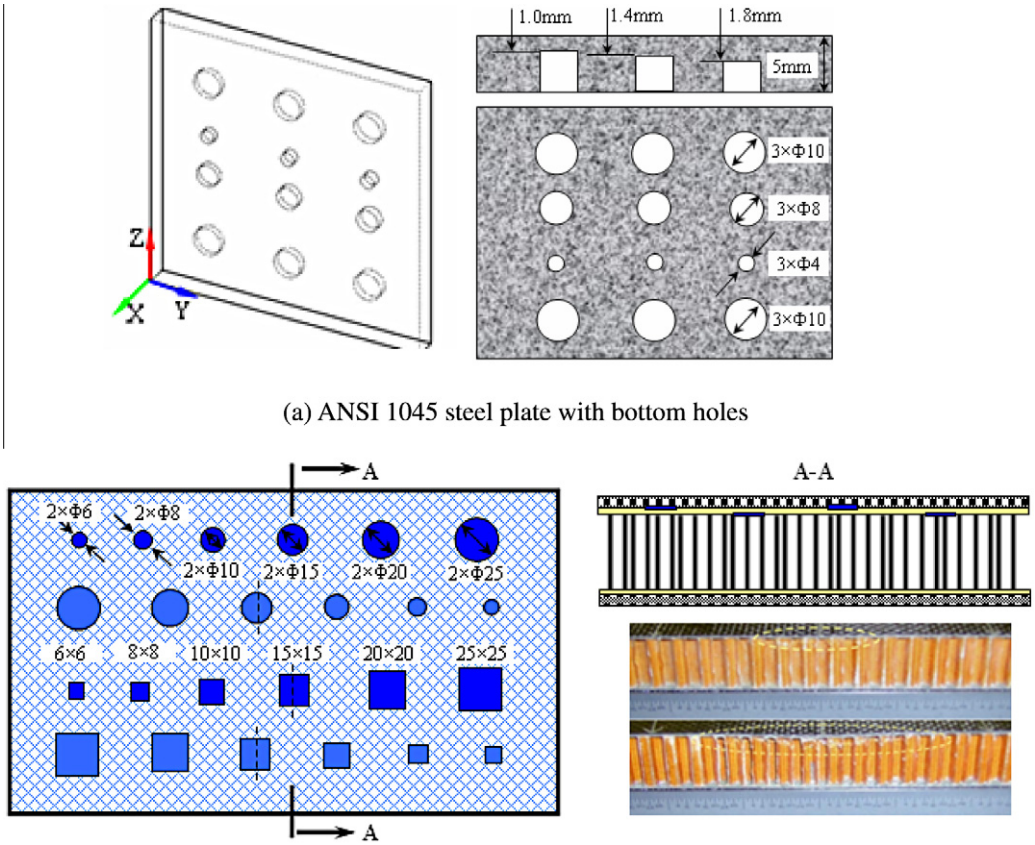

Fig. 8. Specimens structure.

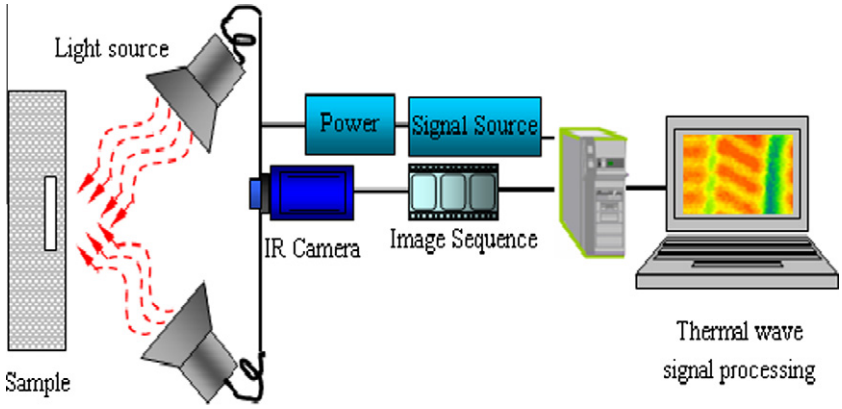

Fig. 9. Schematic diagram of experimental setup.

Fig. 13 shows the phase images of the ANSI 1045 steel plate specimen, using FTM, FPCM and DLICM at modulation frequency f_e = 0.12 Hz.

Fig. 10. Experimental system setup.

Table 1
Experimental parameters of ANSI 1045 steel plate.

Modulated frequency, f_e (Hz)	Sample frequency, f_s (Hz)	Frames	Power (KW)
0.12–0.40	37	1110	1.0

Table 2
Experimental parameters of CFRP honeycomb.

CFRP thickness, h_d (mm)	0.5	1.0	1.5
Modulated frequency, f_e (Hz)	0.4	0.1	0.045
Frames	1110		
Frame rate, f_s (Hz)	37		
Power (KW)	2.0		

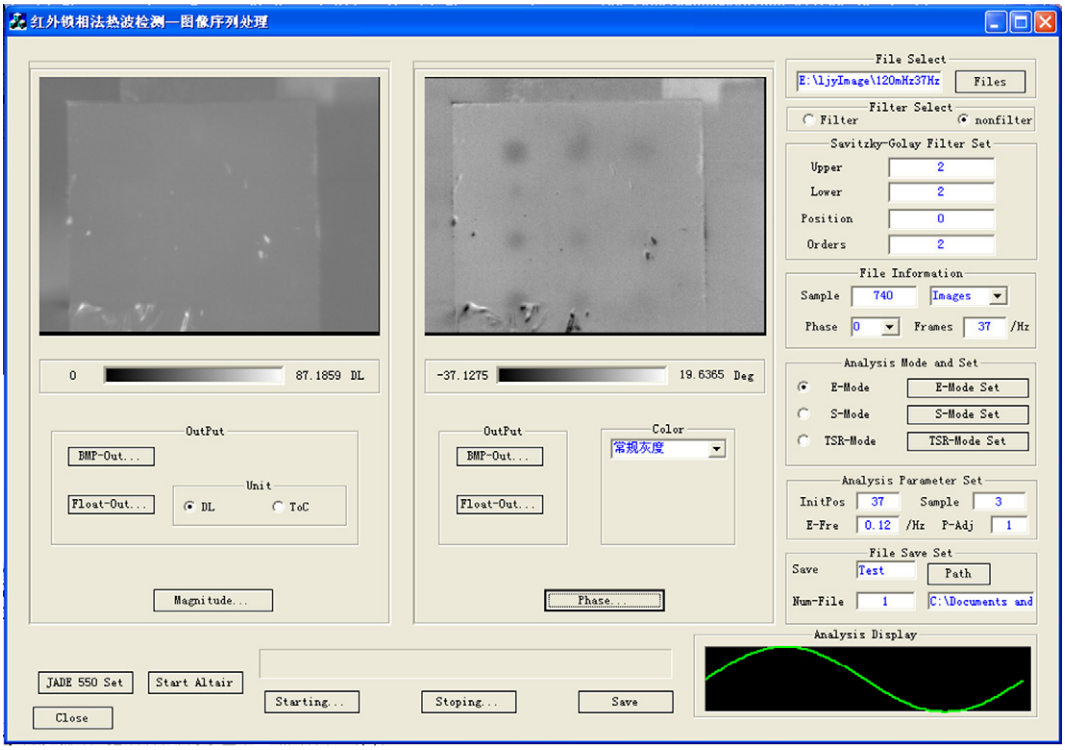

Fig. 11. Thermal wave signal processing software.

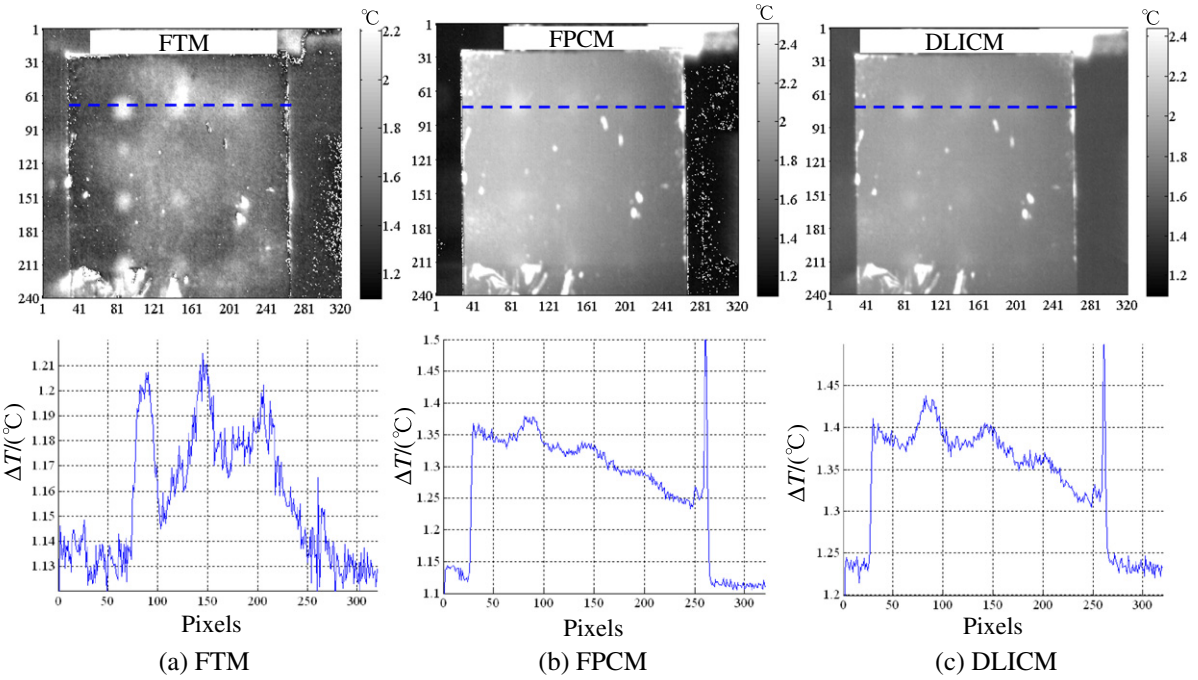

Fig. 12. Amplitude image by various thermal wave signal processing.

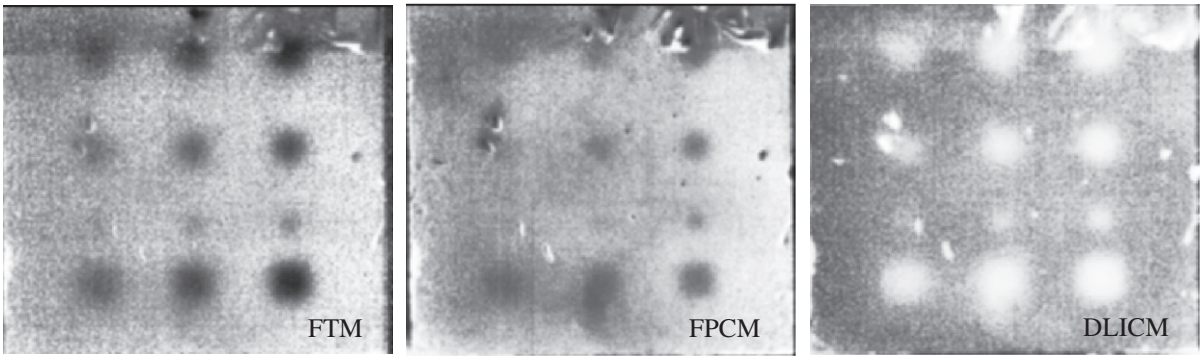

Fig. 13. Phase images by various thermal wave signal processing.

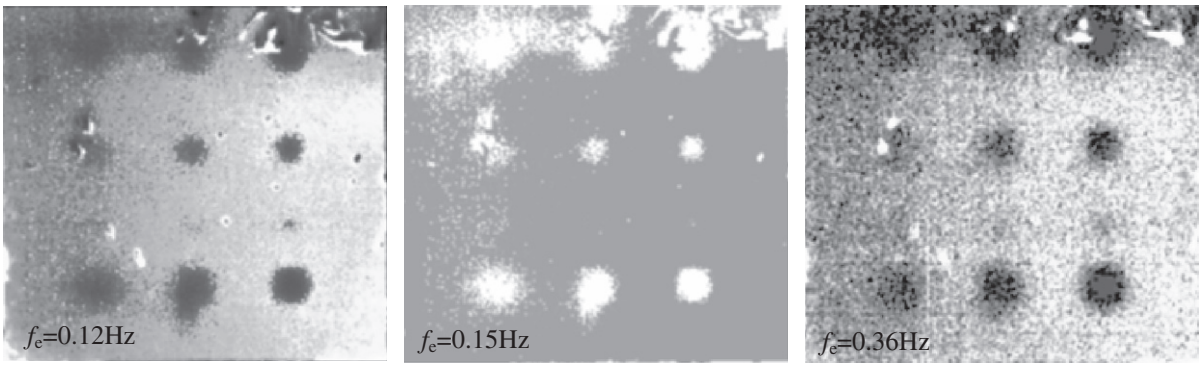

Fig. 14. Experimental results of TCM processing in lock-in.

The results show that the processing methods of thermal wave harmonic components in steady state have different subsurface defect detection capability in-phase image at given modulation frequency. The FTM is applicable for subsurface defect detection of ANSI 1045 carbon steel material, since the phase image presents a better defect shape compared with PFCM and DLICM. However, the PFCM is applicable for thermal wave signal processing with high computation speed for lock-in thermogra-

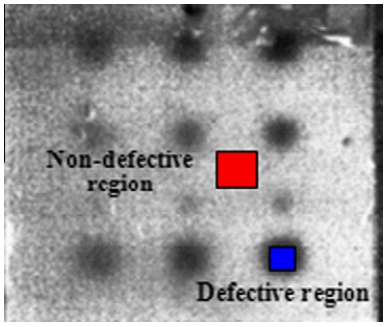

Fig. 15. Defective region and non-defective one.

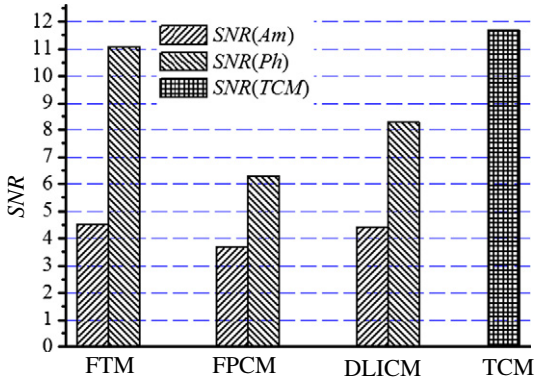

Fig. 16. *SNR*s comparison by different processing algorithms.

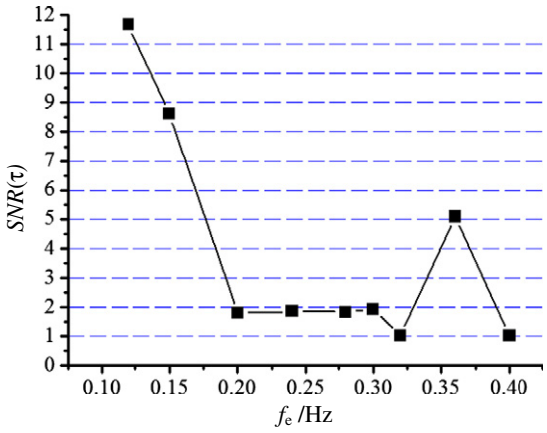

Fig. 17. *SNR* variations vs. modulation frequency by TCM.

phy when the surface temperature reached up to the steady state.

Fig. 14 illustrates the experimental results of the ANSI 1045 steel plate with TCM processing algorithm in lock-in thermography at modulation frequencies $f_e = 0.12$ Hz, $f_e = 0.15$ Hz, and $f_e = 0.36$ Hz, respectively. The experimental results show that the TCM is able to preserve the defect shape. The measurements are also affected by modulation frequencies. However, with an increase of modulation frequency, the signal to noise ratio (SNR) deteriorates.

The *SNR*s defined in Eqs. (29)–(31) are proposed to evaluate the performance of defect detection.

$$SNR(Am) = \frac{\overline{Am_D} - \overline{Am_N}}{\sigma(Am_N)} \tag{29}$$

$$SNR(Ph) = \frac{\overline{Ph_D} - \overline{Ph_N}}{\sigma(Ph_N)} \tag{30}$$

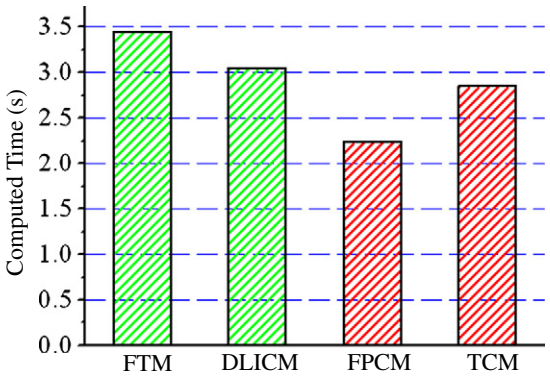

Fig. 18. Computing time comparison for different processing algorithms.

$$SNR(\tau) = \frac{\overline{\tau_D} - \overline{\tau_N}}{\sigma(\tau_N)} \tag{31}$$

where $SNR(Am)$ represents the amplitude SNR in amplitude image, $SNR(Ph)$ represents the phase SNR in-phase image; $\overline{Am_D}$ and $\overline{Ph_D}$ are mean values of amplitude and phase in defective region respectively; $\overline{Am_N}$ and $\overline{Ph_N}$ are mean values of the amplitude and phase in non-defective region respectively; $\sigma(Am_N)$ and $\sigma(Ph_N)$ are the standard deviation of amplitude and phase in non-defective region; $SNR(\tau)$ is the time constant signal–noise-ratio in time constant image; $\overline{\tau_D}$ and $\overline{\tau_N}$ are the time constant mean value in defective region and non-defective region; and $\sigma(\tau_N)$ is the standard deviation of time constant in non-defective region.

The selected defective and non-defective regions are marked in Fig. 15. Fig. 16 shows the comparisons of *SNR*s of amplitude and phase at modulation frequency $f_e = 0.12$ Hz by different processing algorithms for surface temperature in transient state.

It is known from Fig. 16 that the *SNR*s of amplitude and phase are higher by FTM compared to PFCM and DLICM. The *SNR* of PFCM is the lowest by processing thermal wave signal in transient state using lock-in thermography because the amplitude and phase are computed under the hypothesis of the thermal wave signal reaching up to the steady state. However, the transient component of thermal wave signal in transient state is considered as noise signal, so that the *SNR* of PFCM is lowered.

Fig. 17 shows the variation of *SNR* with modulation frequencies by TCM. Fig. 18 illustrates the comparisons of computing times by different processing algorithms using lock-in thermography based on analyzing image sequences in one modulation period.

Fig. 17 shows that the modulation frequency affects the *SNR* of TCM in lock-in thermography, for given ANSI 1045 steel, that the modulation frequency range from 0.12 Hz to 0.15 Hz is available for subsurface detection. From Eq. (28), it can be seen that the modulation period should be selected the same order of magnitude as time constant of a given material for higher *SNR* of TCM. From Fig. 18, the computation time of FPCM is the shortest among all processing algorithms using lock-in thermography based on analyzing image sequences. In one modulation period, FPCM processing method uses only four points to estimate the amplitude and phase of thermal wave harmonic component in steady state, so that, the computation cost is lowered. It can be seen that TCM method proposed in this paper saves the computation cost compare with FTM and DLICM processing method as well.

Fig. 19 shows the phase images of CFRP sheets faces honeycomb specimen with CFRP sheets face thickness $h_d = 0.5$ mm, $h_d = 1.0$ mm and $h_d = 1.5$ mm, using FTM and DLICM at modulation frequencies $f_e = 0.4$ Hz, $f_e = 0.1$ Hz, and $f_e = 0.045$ Hz, respectively.

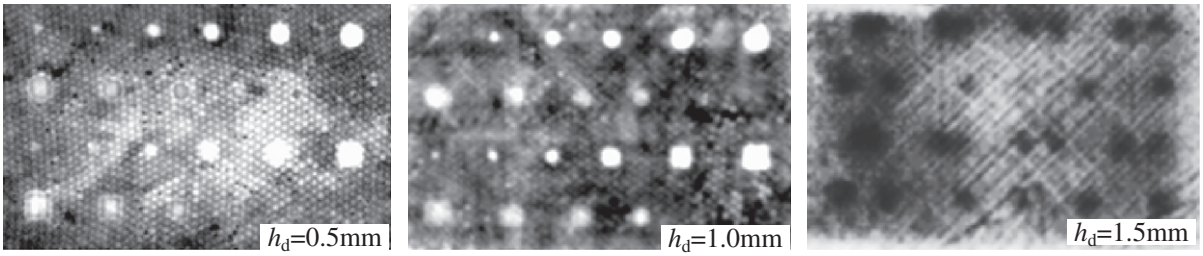

Fig. 19. Phase images of CFRP honeycomb specimens.

Experimental results illustrate that the smallest defects with the diameter of 6 mm can be detected in-phase image for h_d = 0.5 mm and h_d = 1.0 mm at given modulation frequencies by using FTM and DLICM thermal wave processing algorithms in lock-in thermography. The CFRP sheet's face thickness, however, h_d is increased? to 1.5 mm, some smaller size defects are not accurately detected, and the image SNR is decreased in-phase image.

In order to investigate the subsurface defect detectivity by using of pulsed thermography and lock-in thermography, experiments were carried out, which the specimen was selected a CFRP sheet faces honeycomb that the sheet face thickness is 1.5 mm. The modulation frequencies f_e is 0.064 Hz and the frame frequency f_s is 37 Hz by using lock-in thermography. The analysis time is set to 5.4 ms for differential analysis and the frame frequency f_s is selected as 37 Hz by using pulsed thermography.

Fig. 20a shows the amplitude and phase image results obtained by the FTM process by using lock-in thermography. Fig. 20b shows the time constant image by TCM process using lock-in thermography; while Fig. 20c shows the differential image by one order dif-

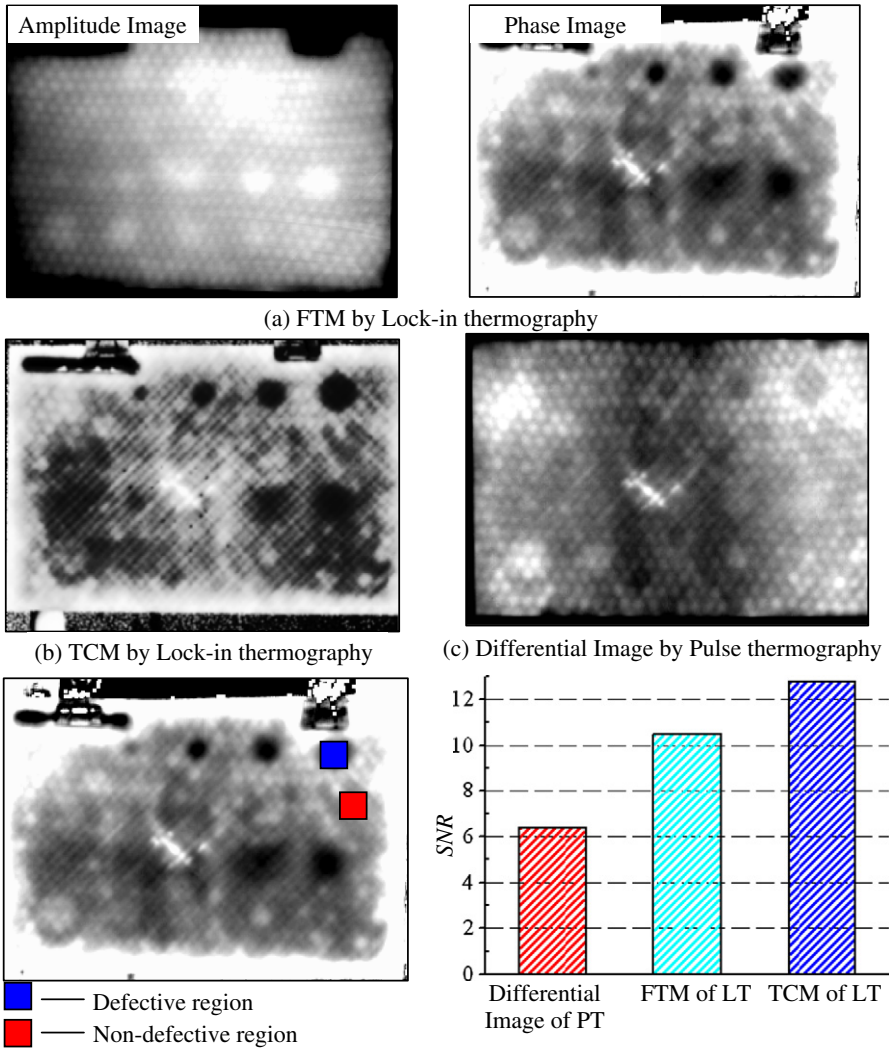

Fig. 20. Results comparison of pulse thermography and lock-in thermography.

ferential process using pulsed thermography. Fig. 20d shows the comparison of SNR on? given defective region and non-defective region by different processing algorithms using lock-in thermography and pulsed thermography.

It can be seen that the contrast of defect is higher by FTM phase image and TCM time constant image using lock-in thermography than differential image using pulsed thermography from Fig. 20a–c. The small-sized defect is easily founded from FTM phase image and TCM time constant image using lock-in thermography. However, the small-sized defect can not be measured from the differential image using pulsed thermography, and this image has lost some details of interface between CFRP sheet face and honeycomb. The TCM process method has higher SNR for CFRP sheet face honeycomb structure than FTM using lock-in thermography and differential process using pulsed thermography from Fig. 20d.

6. Conclusion

In this paper, thermal wave signal processing algorithms are investigated in lock-in thermography. The thermal wave signal harmonic component can be extracted by Fourier transforms method (FTM), four-point correlation method (FPCM) and digital lock-in correlation method (DLICM), which can be used to calculate the amplitude and phase angle of thermal wave signal harmonic component at a given modulation frequency. Time constant method (TCM) is proposed to calculate the thermal wave signal time constant in transient state in lock-in thermography. This method is valuable for non-destructive testing by using lock-in thermography. Experiments confirm that these thermal wave signal processing algorithms are very practical and effective for detection of subsurface defects in lock-in thermography using computer software. IR lock-in thermography system based on analyzing image sequence is an effective technique for non-destructive testing and evaluation.

Acknowledgements

This work was supported by the Chinese National Natural Science Foundation under Contract No.60776802, the Fundamental Research Funds for the Central Universities under Contract No. HIT.NSRIF.2009025, the 111 Project (B07018) and the Heilongjiang Provence Project under Contract No. GB06A512.

References

[1] X.P. Maldgue, Theory and practice of infrared technology for nondestructive testing, in: K. Chang (Ed.), Wiley Series in Microwave and Optical Engineering, Wiley, New York, 2001, p. 684.
[2] Clemente Ibara-Castanedo, Marc Genset, et al. Inspection of aerospace materials by pulse thermography, lock-in thermography and virbothermography: a comparative study, in: Thermosense XXIX, Proc. of SPIE, vol. 6541(9), 2007, p. 654116-1.
[3] Ravibabu Mulaveessala, Suneet Tuli, Theory of frequency modulated thermal wave imaging for nondestructive subsurface defect detection, Applied Physics Letters 89 (2006) 191913-3.
[4] X. Maldague, S. Marinetti, Pulse phase infrared thermography, Journal of Applied Physics 79 (5) (1996) 2694–2698.
[5] G. Busse, D. Wu, W. Karpen, Thermal wave imaging with phase sensitive modulated thermography, Journal of Applied Physics 71 (1992) 3962–3965.
[6] O. Brcitenstein, M. Langenkmp, Lock-in Thermography Basics and Use for Functional Diagnostics of Electronic Components. Springer Series in Advanced Microelectronics, Springer-Verlag, Berlin, Heidelberg, 2003.
[7] J.P. Holman, Heat Transfer, Chinese Machine Press, 2005.
[8] Guang-Shu Hu, Digital Signal Processing Theory, Algorithms and Realization, Tsing Hua University Publishing, 2003.
[9] Junyan Liu, Jingmin Dai, Wang Yang. An IR Lock-in Thermography Nondestructive Test System Based on the Image Sequence Processing. 17WCNDT, Shang Hai, China, 2008. <http://www.ndt.net>.